molecules

MDPI

Article

A Comprehensive Experimental and Theoretical Study on the $[\{(\eta^5\text{-}C_5H_5)_2Zr[P(\mu\text{-}PNEt_2)_2P(NEt_2)_2P]\}]_2O$ Crystalline System

Agnieszka Łapczuk-Krygier [1,*], Katarzyna Kazimierczuk [2], Jerzy Pikies [2] and Mar Ríos-Gutiérrez [3,*]

[1] Institute of Organic Chemistry and Technology, Krakow University of Technology, Warszawska St. 24, 31-155 Krakow, Poland
[2] Department of Inorganic Chemistry, Faculty of Chemical, Gdansk University of Technology, G. Narutowicza St. 11/12, 80-233 Gdansk, Poland; katarzyna.kazimierczuk@pg.edu.pl (K.K.); jerpikie@pg.edu.pl (J.P.)
[3] Department of Organic Chemistry, University of Valencia, Dr. Moliner 50, 46100 Valencia, Spain
* Correspondence: a.lapczuk@pk.edu.pl (A.Ł.-K.); rios@utopia.uv.es (M.R.-G.)

Abstract: The structure of tetraphosphetane zirconium complex $C_{52}H_{100}N_8OP_{10}Zr_2$ **1** was determined by single crystal X-ray diffraction analysis. The crystal belongs to the monoclinic system, space group P21/c, with a = 19.6452(14), b = 17.8701(12), c = 20.7963(14)Å, $\alpha = \gamma = 90°$, $\beta = 112.953(7)°$, V = 6722.7(8)Å3, Z = 4. The electronic structure of the organometallic complex has been characterized within the framework of Quantum Chemical Topology. The topology of the Electron Localization Function (ELF) and the electron density according to the Quantum Theory of Atoms in Molecules (QTAIM) show no covalent bonds involving the Zr atom, but rather dative, coordinate interactions between the metal and the ligands. This is the first reported case of a Zr complex stabilized by an oxide anion, anionic cyclopentadienyl ligands and rare tetraphosphetane anions.

Keywords: X-ray crystal structure; zirconocene; phosphetane; ELF; QTAIM

Citation: Łapczuk-Krygier, A.; Kazimierczuk, K.; Pikies, J.; Ríos-Gutiérrez, M. A Comprehensive Experimental and Theoretical Study on the $[\{(\eta^5\text{-}C_5H_5)_2Zr[P(\mu\text{-}PNEt_2)_2P(NEt_2)_2P]\}]_2O$ Crystalline System. *Molecules* **2021**, *26*, 7282. https://doi.org/10.3390/molecules26237282

Academic Editors: Enrico Bodo and Stéphane Bellemin-Laponnaz

Received: 3 October 2021
Accepted: 25 November 2021
Published: 30 November 2021

1. Introduction

This work is a continuation of our comprehensive study of phosphorous complexes. The chemistry of the metalocenes with phourous ligands is very interesting, but, unfortunately, their chemical properties are still rather poorly known. The metallocenes bearing one or two cyclopentadienyl ligands are an important class of the new generation of polymerization catalysts for ethylene polymerization [1–4], asymmetric imine reduction [5], atom transfer radical polymerization [6,7], the dehydrocoupling of dimethylamineborane [8] and imine hydrogenation [9].

The structure and bonding properties of metallocenes and phosphoroorganic molecules have recently received much attention. Although a number of zirconocene complexes with phosphorous ligands have been reported [10], there have been no reports on the structural characterization of compounds with oxygen links, despite those of the polyphosphorus derivatives being known.

Reactions of lithium derivatives of diphosphanes $R_2PP(SiMe_3)Li$ with zirconocenes lead to the formation of phosphanylophosphinidene (R_2P-P) and phosphanylphosphido (R_2P-(R′)P) complexes. It has been shown that thermal decomposition of phosphanylphosphido complexes yields polyphosphorus compounds [11] and if R = Et_2N or iPr_2N, it leads to different phosphetanes [12]. The reactivity of alkali metal phosphides towards zirconocenes has been the subject of thorough studies [11–14].

Here, we report on interesting an dimeric complex, $[\{(\eta^5\text{-}C_5H_5)_2Zr[P(\mu\text{-}PNEt_2)_2P(NEt_2)_2P]\}]_2O$ (**1**), with two phosphetane moieties and two zirconocene groups (Figure 1). Formation of polyphosphorus complexes was earlier observed [11,14], but complexes of phosphetanes as ligands in transition metals complexes are very rare.

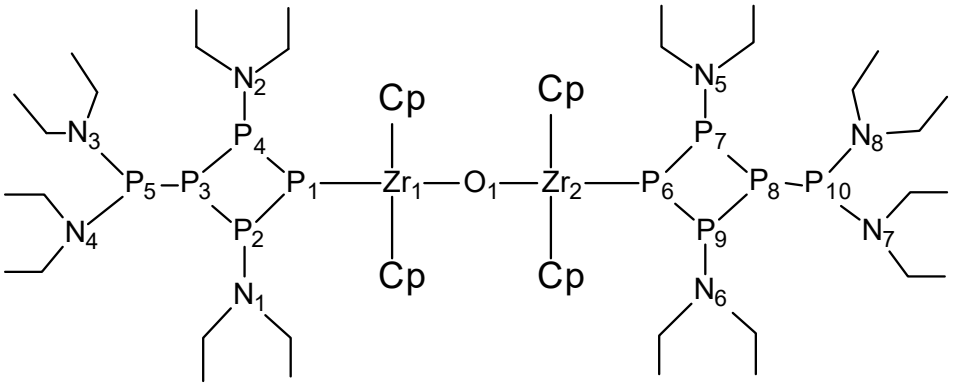

Figure 1. Structure of [{(η^5-C_5H_5)$_2$Zr[P(μ-PNEt$_2$)$_2$P(NEt$_2$)$_2$P]}]$_2$O (**1**).

2. Results and Discussion

2.1. Synthesis and X-ray Study

Our previous research [12,15] has focused on reactions of [Cp_2ZrCl_2] with lithium derivatives of diphosphanes $R_2PP(SiMe_3)Li$. We have confirmed the substitution of one or two chlorido ligands and formation of phosphanylphosphido (R_2P-(Me_3Si)P) or phosphanylophosphinidene (R_2P-P) complexes with a zirconocene group. For R = Et_2N or $^iPr_2N$, the phosphanylphosphido complexes are not always stable, and in reaction solutions, different phosphetanes can be found. Scheme 1 [12] shows the similar reaction of [Cp_2HfCl_2] with $(Et_2N)_2$P-P($SiMe_3$)Li, yielding almost solely the related phosphetane $Et_2NP(PSiMe_3)_2PNEt_2$.

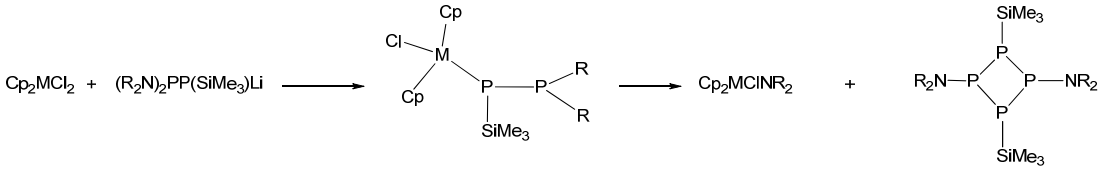

Scheme 1. Reactions of lithium derivatives of diphosphanes $(Et_2N)_2PP(SiMe_3)Li$ with metalocene dichloride (M = Hf, R = Et_2N), yielding a phosphanylphosphido ($(Et_2N)_2$P-(Me_3Si)P) complex, whose thermal decomposition leads to tetraphosphetane.

Reactions of $CpZrCl_3$ with $(R_2N)_2$P-P(SiMe3)Li (R = Et or ^{i}Pr) yield a variety of phosphetanes: $R_2NP(PSiMe_3)_2PNR_2$, R_2NP-$P(PSiMe_3)_2$P-PNR_2 and R_2NP-$P(PNR_2)_2$ $PSiMe_3$ [12]. It should be stressed that the formation of $R_2NP(PSiMe_3)_2PNR_2$ can be easy rationalized in terms of Scheme 1 and very likely involves an intermediate phosphanylphosphido complex. The formations of R_2NP-$P(PSiMe_3)_2$P-PNR_2 and R_2NP-$P(PNR_2)_2PSiMe_3$ are more complicated. Recently, unexpected $^iPr_2NP$-$P(PN^iPr_2)_2PSiMe_3$ was formed in high yield in a reaction of [NacNacFe(μ-Cl)$_2$Li(DME)$_2$] with ($^iPr_2N)_2PP(SiMe_3)$Li. The side products, $P(SiMe_3)_3$ and $(^iPr_2N)_2PP(N^iPr_2)_2$, pointed to the oxidation of $(^iPr_2N)_2PP(SiMe_3)$Li involving the TM complex as a driving force of this reaction [15].

Dimeric complex **1** incorporated two $ZrCp_2$ moieties in one molecule, although CpCp*$ZrCl_2$ was used as a starting complex. There was likely an initial rearrangement in the reaction mixture prior to the phosphetane $(Et_2N)_2PP(PNEt_2)_2PSiMe_3$ formation. In our studies, we often isolate Cp_2ZrCl_2 from the reaction mixture while only CpCp*$ZrCl_2$ is used in the reaction (1)

$$2\ Cp^*CpZrCl_2 \rightarrow Cp_2ZrCl_2 + Cp^*_2ZrCl_2 \quad (1)$$

The next step is the reaction of (Cl)Cp_2Zr-O-$ZrCp_2$(Cl) with the phosphetane and an excess of $(Et_2N)_2PPSiMe_3$(Li) yielding complex **1**, LiCl and $(Et_2N)_2PP(SiMe_3)_2$ (Scheme 2).

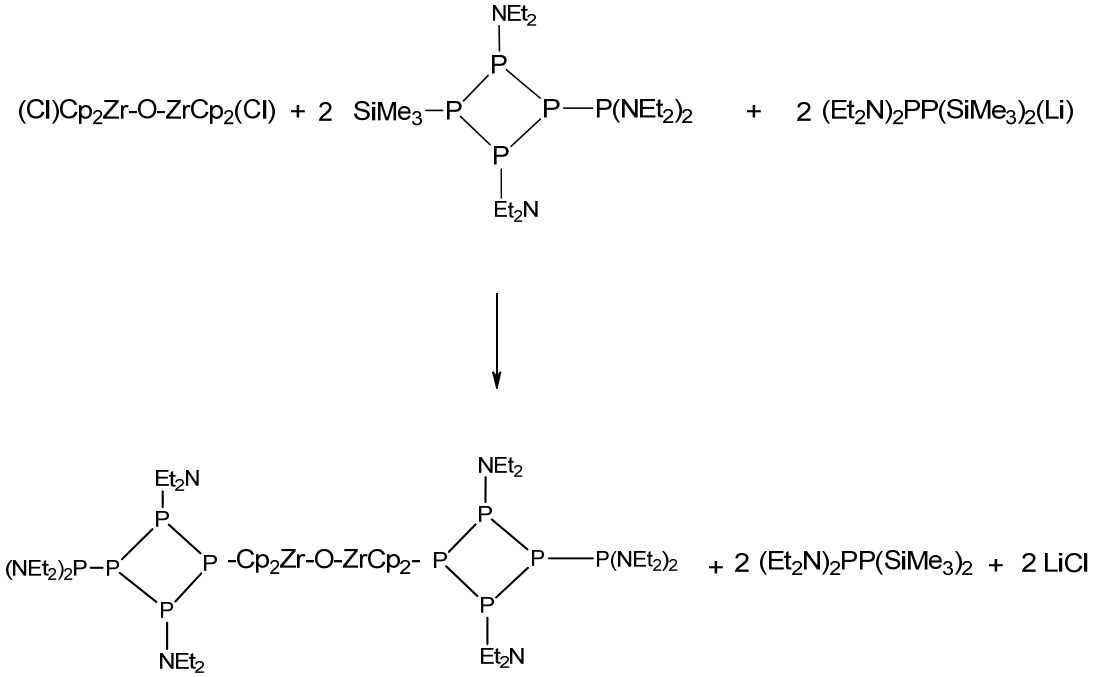

Scheme 2. Reaction of (Cl)Cp_2Zr-*O*-ZrCp_2(Cl) with the phosphetane and an excess of $(Et_2N)_2PPSiMe_3$(Li) yielding complex **1**, LiCl and $(Et_2N)_2PP(SiMe_3)_2$.

Experiments with Cp*$CpZrCl_2$ have shown that it is far less reactive than Cp_2ZrCl_2 towards lithium salts of diphosphanes and it likely did not react.

The Zr-O-Zr moiety more likely originates from the decomposition of THF by zirconium compounds or from hydrolysis with traces of water of zirconocene dichloride. Similar compounds were obtained by subjecting a solution of zirconocenederivatives in a toluene–hexane mixture to slow hydrolysis in air [16,17], or they can be prepared from µ-oxo dichloride complexes [{$Cp_2Zr(Cl)$}$_2$O] [18]. These compounds are very susceptible to hydrolysis and the formation of coordination polymers.

The study of a reaction solution with ^{31}P-NMR displayed a complicated mixture of partially not identified species and indicated that $Et_2NP(PSiMe_3)_2PNEt_2$ was not formed; thus, the reaction similar to Scheme 1 did not proceed.

The molecular structure of **1** shown in Figure 2 consists of two nearly identical (η^5-C_5H_5)$_2$Zr molecular units linked together by an oxygen. The oxygen occupies one of four metal coordination sites, and with the polyphosphorus group and the two centroids of the cyclopentadienyl rings, completes a distorted tetrahedral geometry around each zirconium center (Figure 3).

The $Cp_{centroid}$-Zr-$Cp_{centroid}$ angle of 131.0° is normal for zirconocene complexes, and the average Zr-$Cp_{centroid}$ distance of 2.21 Å is comparable with those of other derivatives. The angle between Zr-O-Zr depends on the R-group (Tables 1 and 2).

Table 1. Bond angles between Zr-O-Zr and Zr-O distance in [(η^5-C_5H_5)$_2$Zr]$_2$O.

Compound	M-O (Å)	O-M-O (°)	Ref.
{(η^5-C_5H_5)$_2$Zr[P(µ-$PNEt_2$)$_2$P(NEt_2)$_2$P]}$_2$O	1.960(4) 1.955(4)	179.3(3)	This work
[(η^5-C_5H_5)$_2$Zr(SC_6H_5)]$_2$O	1.968(3) 1.964(3)	165.8(2)	[16]
[(η^5-C_5H_5)$_2$Zr(NCO)]$_2$O	1.949(3) 1.942(3)	165.7(2)	[19]
[(η^5-C_5H_5)$_2$Zr(OC(OtBu)=CMe_2)]$_2$O	1.966(1) 1.972(1)	174.9(1)	[18]

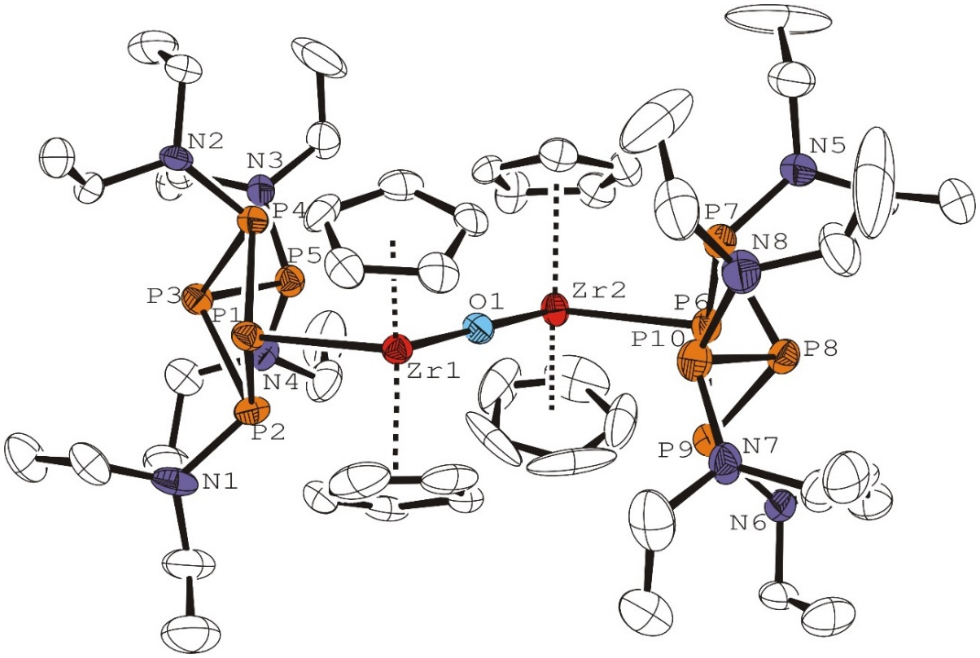

Figure 2. ORTEP3 drawing of the title compound (ellipsoids for non-H atoms are drawn at the 50% probability level).

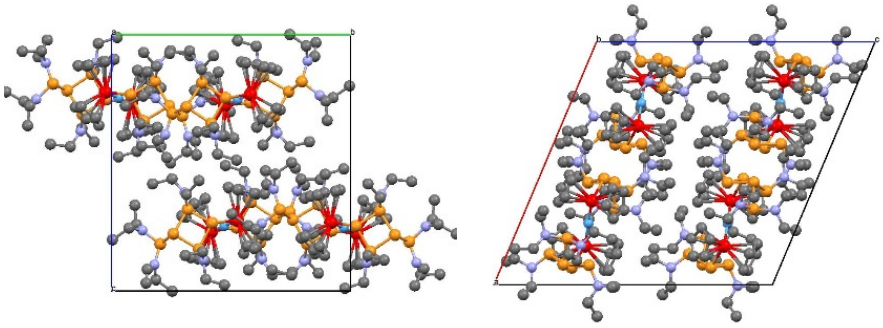

Figure 3. The crystal packing of the title complex, viewed along a and b axes.

The phosphorous skeleton indicates a butterfly structure similar to 2,4-bis[bis (diisopropylamino)phosphanyl]-1,2,3,4-tetraphosphabicyclo- [1.1.0]butane [14]. The distances between the centers of cyclopentadienyl rings and zirconium atoms are 2.235 Å and 2.247 Å for (Zr1) and 1.251 Å, 2.251 Å and 2.245 Å for (Zr2). The angles between Cp-centroids and atoms are 129.395° in Cp_2Zr1 and 128.10° in Cp_2Zr_2 (Tables 3 and 4).

2.2. Theoretical Study

Although the nuclei position and cristallographic data of complex **1** have been clearly characterized by X-ray crystallography, the nature of the chemical bonding in its framweork remains unknown. Thus, in order to gain some insight into the electronic structure and bonding pattern of complex **1**, the geometry of a reduced computational model **1′** in which the ethyl groups at **1** were substituted by hydrogen atoms was first optmized and compared to both experimetal and theoretical data of **1**. Then, the bonding pattern of model complex **1′** was characterized within the Quatum Chemical Topology [20] perspective, through the topological analysis of the electron localization function (ELF) [21] and the electron density, by means of the Quantum Theory of Atoms in Molecules (QTAIM) [22–24].

Table 2. Crystallographic characteristics and the X-ray data collection and structure-refinement parameters for $C_{52}H_{100}N_8OP_{10}Zr_2$.

Empirical Formula	**$C_{52}H_{100}N_8OP_{10}Zr_2$**
Formula weight	1345.54
Temperature/K	120(2)
Wavelength/Å	0.71073 (Mo K_α)
Crystal system	monoclinic
Space group	$P\,2_1/n$
a/Å b/Å c/Å	19.6452(14) 17.8701(12) 20.7963(14)
α/deg β/deg γ/deg	90 112.953(7) 90
V/Å ^{3}	6722.7(8)
Z	4
D_c/Mg m^{-3}	1.329
μ/mm^{-1}	0.588
F(000)	2824
Crystalsize/mm	0.0673 × 0.0423 × 0.0141
Θrange/deg	2.25 to 25.5
Index ranges	$-21 \leq h \leq 23$ $-21 \leq k \leq 21$ $-25 \leq l \leq 23$
Reflections collected/unique	47963/12510[R(int) = 0.1454]
Data/restraints/parameters	12510/0/658
Goodness of fit on F^2	0.805
Final R indices [I>2σ(I)]	R_1 = 0.0523 $w\,R_2$ = 0.1382
R indices (all data)	R_1 = 0.0993 $w\,R_2$ = 0.1535
Largest diff. peaks [e Å $^{-3}$]	0.117, −0.947

Table 3. Selected bond lengths (d, Å).

Zr1 O1	1.960(4)	Zr2 O1	1.955(4)
Zr1 P1	2.652(2)	Zr2 P6	2.662(2)
P1 P2	2.210(2)	P6 P9	2.205(3)
P1 P4	2.203(3)	P6 P7	2.208(3)
P2 P3	2.238(3)	P9 P8	2.247(3)
P4 P3	2.245(3)	P7 P8	2.236(3)
P5 P3	2.222(3)	P8 P10	2.228(3)
P2 N1	1.701(9)	P9 N6	1.717(5)
P4 N2	1.697(5)	P7 N5	1.706(7)
P5 N4	1.698(7)	P10 N8	1.695(7)
P5 N3	1.703(6)	P10 N7	1.698(6)

Table 4. Selected bond angles (ω, deg).

Zr1 O1 Zr2	179.3(3)	P4 P3 P2	88.2(1)	P6 P7 P8	85.5(1)
O1 Zr1 P1	103.0(1)	Zr1 P1 P2	110.15(9)	P8 P9 P6	85.3(1)
P2 P1 P4	90.0(1)	Zr1 P1 P4	107.52(9)	P9 P8 P7	87.9(1)
P1 P4 P3	85.07(9)	O1 Zr2 P6	103.1(1)	Zr2 P6 P7	109.03(9)
P3 P2 P1	85.1(1)	P9 P6 P7	89.7(1)	P9 P6 Zr2	108.58(9)

2.3. Geometrical Analysis of Complex **1** *and Reduced Model* **1′**

In order to check the suitability of reduced model **1′** to represent the bonding pattern of complex **1**, the X-ray and ωB97X-D/Def2TZV geometries of the main motif of **1** and the ωB97X-D/Def2TZV-optimized geometry of reduced model **1′** were compared. Table 5 gathers the most relevant data, namely the distances between each Zr atom and the surrounding tetraphosphetane, cyclopentadienyl and oxygen systems, while Figure 4 displays the optimized geometry of reduced model **1′**.

Table 5. Most relevant X-ray and ωB97X-D/Def2TZV geometrical data of the main motif of complex **1** and reduced model **1′**.

Structure	**1**		**1′**
Method	**X-ray**	**DFT**	**DFT**
d(Zr1-Cp1)	2.500	2.527	2.527
d(Zr1-Cp2)	2.499	2.512	2.525
d(Zr2-Cp3)	2.509	2.511	2.525
d(Zr2-Cp4)	2.471	2.530	2.527
d(Zr1-O)	1.960	1.968	1.969
d(Zr2-O)	1.955	1.969	1.969
d(Zr1-P)	2.652	2.675	2.681
d(Zr2-P)	2.662	2.670	2.681
a(Zr1-O-Zr2)	179.3	177.5	180.0
a(O-Zr1-P)	103.0	103.6	103.7
a(O-Zr2-P)	103.1	104.1	103.7
a(O-Zr1-Cp1)	113.2	114.3	114.1
a(O-Zr1-Cp2)	109.0	109.8	113.5
a(O-Zr2-Cp3)	112.5	110.9	113.4
a(O-Zr2-Cp4)	106.6	87.7	114.2

As can be observed from Table 5, the most remarkable difference between the experimental and the computed geometries is that the distances are slightly shorter in the former as a consequence of the crystal packing. The DFT-optimized geometry of **1** is very similar to the experimental one; the Zr-X (with X = Cp, P or O) distances differ by 0.06 Å at most and three of the four O-Zr-Cp angles vary by less than 2°. On the other hand, the geometry of the reduced model **1′** is almost equivalent to the DFT geometry of **1**; the most relevant distances change by less than 0.02 Å. When compared to the experimental data, the geometry of the reduced model **1′** fits, as well as the DFT geometry of **1**, and even improves some of the angles. Consequently, these data show that the reduced model **1′** can be used as a representative case study to illustrate the bonding pattern of **1**.

2.3.1. ELF Topological Analysis of **1′**

The quantum chemical analysis of Becke and Edgecombe's ELF [25] is an appealing procedure that provides a straightforward connection between the electron density distribution and the chemical structure [26,27]. Thus, in order to shed light onto the bonding characteristics of complex **1**, the ELF of **1′** was topologically analyzed. The ELF attractor positions of the core and valence basins of **1′** are shown in Figure 5, the most relevant valence basin populations are given in Table 6 and 2D color-filled maps of the ELF are represented in Figure 6.

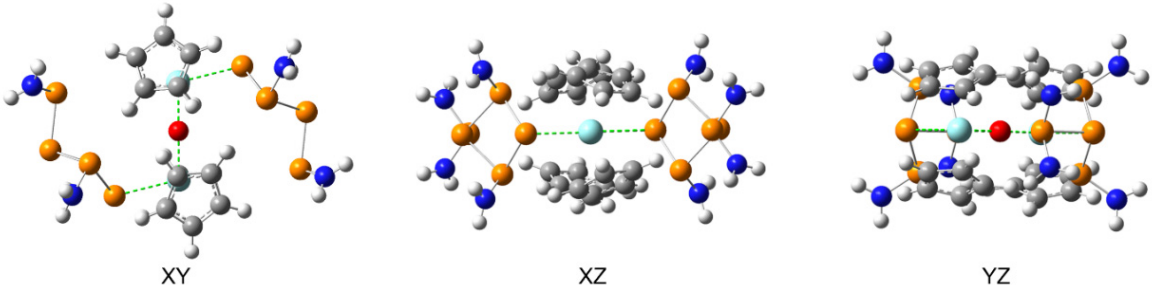

Figure 4. Views of the ωB97X-D/Def2TZV gas phase-optimized geometry of model **1′** along planes XY, XZ and YZ.

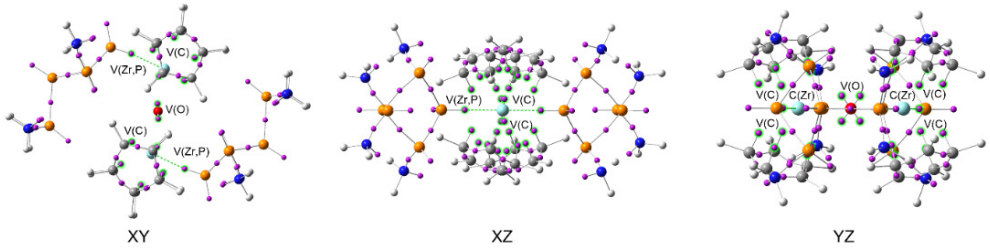

Figure 5. ELF attractor positions of the core and valence basins of **1′** viewed along planes XY, XZ and YZ. Relevant attractors are highlighted in green.

Table 6. Average populations, $\overline{N}$, in average number of electrons, $\bar{e}$, associated with the ELF basins of **1′**. Subscript "t" refers to the total population of equivalent basins.

ELF Basins	$\overline{N}$	ELF Basins	$\overline{N}$
C(O)	2.11	C(P)	10.08
V_t(O)	7.48	C(N)	2.11
C(Zr)	37.34	V(P)	2.24
V(Zr,P)	1.95	V(N)	1.78
C(C)	2.09	V(P,P)	1.78
V_t(C)	1.21	V(N,P)	1.94
V(C,C)	2.64		

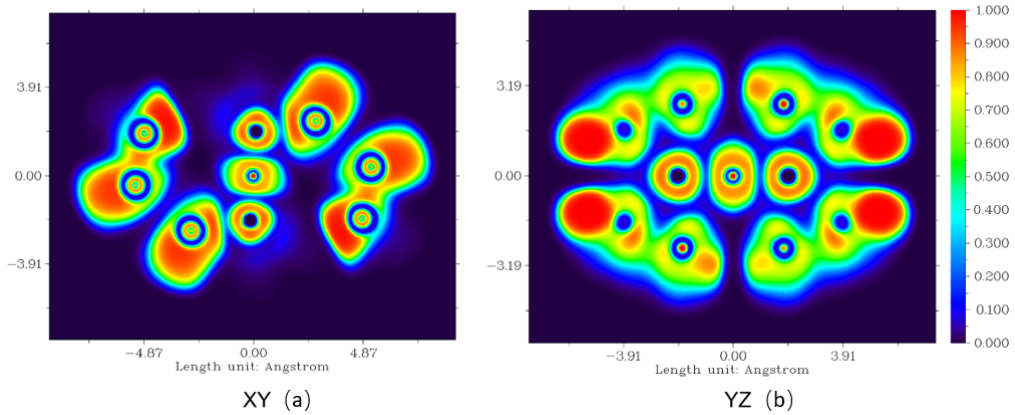

Figure 6. Color-filled maps of the ELF of **1′** along planes XY (**a**) and YZ (**b**).

Within the ELF context, monosynaptic basins, labelled V(A), are associated with non-bonding regions, while disynaptic basins, labelled V(A,B), connect the core of two nuclei A and B and thus correspond to a bonding region between A and B [28]. The topological analysis of the ELF of **1′** shows the presence of four V(O) monosynaptic basins integrating a total population of 7.48 e, two C(Zr) core basins integrating 37.34 e, five V(C) monosynaptic basins integrating an average total population of 1.21 e at each Cp ring and two V(Zr,P)

disynaptic basins integrating 1.95 e (see Table 6). Therefore, the ELF basin synapticities and populations suggest the presence of an O^{2-} oxide anion, four Cp^{1-} anions and two Zr^{2+} cations, which seem to be covalently bound only to the closer P phosphorus atom of the contiguous tetraphosphetane systems.

In order to further ascertain the ELF bonding pattern of **1′**, the 2D color-filled maps of the ELF along planes XY and YZ are represented in Figure 6. The 2D color-filled map along plane XY emphasizes the P-Zr1-O-Zr2-P system (Figure 6a), while the one along plane YZ highlights the Cp_2-Zr1-O-Zr2-Cp_2framework (Figure 6b). Both Figure 6a,b show that the aformentioned sets of nuclei are separated from each other by light blue color regions associated with very low ELF values of 0.1–0.2, which means that there are no covalent interactions between them. Interestingly, Figure 6b also evidences the polarized structure of the Cp anions towards the Zr cations and the different shape of the ELF domains depending on the nuclei nature. In this sense, the deformation of the ELF domains of the O and P nuclei around the Zr nucleus is noteworthy.

These pictures suggest that there is no covalent Zr-P bond, despite the disynaptic assignation of the V(Zr,P) basin between the P and Zr nuclei, thus emphasizing the need for a deeper analysis.

2.3.2. QTAIM Analysis of **1′**

In order to complement the topological analysis of the ELF and clarify the bonding pattern of **1′**, the topology of the electron density distribution was analyzed within the QTAIM [23,24]. The evaluation of the sign of the Laplacian of the electron density in combination with other indicators at the bonding critical points (BCPs), such as the electron density (ρ_{cp}), the Lagrangian kinetic energy (G_{cp}) and the local energy density (H_{cp}), can offer a valuable insight into the the types of bonds that they are signatures of. Table 7 provides a summary of the topological indicators and features that characterize the atomic interactions [25].

The atomic interactions can be classified [26–28] as open-shell (shared) interactions ($\nabla^2\rho_{cp} < 0$, $H_{cp} \ll 0$), transit (intermediate) interactions ($\nabla^2\rho_{cp} > 0$, $H_{cp} < 0$) and closed-shell interactions ($\nabla^2\rho_{cp} > 0$, $H_{cp} > 0$). Open-shell interactions involve covalent and polar covalent bonds [27,29]; intermediate interactions are partially covalent interactions which include coordinate (dative) bonds, strong hydrogen bonds, metallic bonds, etc. [26,29,30]; and closed-shell interactions include ionic bonds and weak intermolecular interactions, such as weak and medium hydrogen bonds, van der Waals interactions, etc. [26,29].

Table 7. Topological indicators and features that characterize the atomic interactions.

	ρ_{cp}	$\nabla^2\rho_{cp}$	G_{cp}/ρ_{cp}	H_{cp}
Open-shell (covalent bonds)	Large	<0	<1	<0
Intermediate	Large	Arbitrary	≥1	<0
Polar covalent bond	Large	<0	>1	<0
Dative bond	Small	≥0	~1	≤0
Metallic bond	Small	~0	≤1	≤0
Closed-shell (ionic bonds)	Small	>0	≥1	>0

Additionally, atomic interactions can be classified by the bond degree parameter $BD = H_{cp}/\rho_{cp}$ (the total energy per electron at BCP) [27,28]. For non-covalent closed-shell interactions, the BD parameter is positive and indicates a softening degree (SD): the weaker and more closed-shell in nature the interactionis, the greater the SD magnitude. For shared and intermediate (partially covalent) interactions, the BD parameter is negative and indicates the covalence degree (CD) of the interactions, i.e., the stronger and more covalent the interactions are, the greater the CD magnitude.

The value of electron density at BCP is also an important characteristic [23,31]. Covalent interactions exhibit $\rho_{cp} > 0.14$ a.u. [26], partially covalent (intermediate) interactions

are characterized by $0.04 < \rho_{cp} < 0.12$ a.u. [26,32] and closed-shell (electrostatic) interactions are characterized by $\rho_{cp} < 0.04$ a.u. [33].

The balance between the kinetic electron energy density G_{cp} and the potential electron energy density V_{cp} has been also used to reveal the nature of interactions. If $|V_{cp}|/G_{cp} > 2$, then the interaction is covalent in nature; if $1 < |V_{cp}|/G_{cp} < 2$, then the interaction is only partially covalent; and if $|V_{cp}|/G_{cp} < 1$, then the nature of the interaction is purely non-covalent [30].

The QTAIM topological indicators at the BCP associated with the Zr-P (BCP1), Zr-O (BCP2) and Zr-Cp (BCP3) regions of **1′** are gathered in Table 8, while Figure 7 shows the contour-line maps of the Laplacian of the electron density $\nabla^2\rho_{cp}$ of **1′** on the molecular planes XY and YZ. Note that only these regions have been considered as there is no ambiguity about the pure covalent character of the Cp C-C and C-H bonds and the tetraphosphetane P-P, P-N and N-H bonds. The three BCPs present $\nabla^2\rho_{cp} > 0$, $H_{cp} < 0$ and $0.04 < \rho_{cp} < 0.12$ a.u., indicating that the interactions involving the Zr atom are intermediate interactions between typical covalent and ionic bonds. In addition, Table 7 provides a way to distinguish between different types of intermediate interactions. Thus, the $\nabla^2\rho_{cp} > 0$, the $G_{cp}/\rho_{cp} \sim 1$ and the $H_{cp} \sim 0$, together with the discard of any metallic bond, suggest that the considered interactions correspond to dative or coordinate bonds. According to the BD parameter, both Zr-P (BD = −0.26) and Zr-O (BD = −0.22) dative bonds have more covalent character than the Zr-Cp coordinate bond (BD = −0.10). Indeed, the $|V_{cp}|/G_{cp}$ quantity suggests that while both Zr-P and Zr-O interactions fit well as partial covalent interactions, the Zr-Cp one is on the borderline between intermediate and ionic interactions.

On the other hand, delocalization indices (DI) provide a measure of the Fermi correlation shared between atomic basins and hence of the number of electrons shared. The DI values for complex **1′** are given in Table 8. As can be observed, the DI values increase in the order Zr-P < Zr-O < Zr-Cp, indicating a higher shared density between the Zr and Cp. This tendency contrasts with the inverse covalency trend characterized by the BD and $|V_{cp}|/G_{cp}$ indicators, which suggest an almost ionic Zr-Cp interaction, but can be explained by the fact that the sum of DI between Zr and the five C and H atoms of Cp is considered; the DI at one single BCP between Zr and one of the Cp carbon atoms is 0.208. The higher DI in Zr-O than in Zr-P, despite its lower BD, can also be explained by the higher electronegativity of the oxide anion, which might polarize the density of the Zr cation more into the former region.

Table 8. QTAIM topological indicators at the BCP associated with the Zr-P, Zr-O and Zr-Cp regions at **1′**. ρ_{cp} is given in e·Å^{-3}, $\nabla^2\rho_{cp}$ in e·Å^{-5}, and H_{cp}, G_{cp} and V_{cp} in hartree·Å^{-3}.

	ρ_{cp}	$\nabla^2\rho_{cp}$	G_{cp}/ρ_{cp}	H_{cp}	H_{cp}/ρ_{cp}	$\lvert V_{cp}\rvert/G_{cp}$	DI
BCP1 (Zr-P)	0.058	0.044	0.453	−0.015	−0.262	1.578	0.564
BCP2 (Zr-O)	0.119	0.524	1.311	−0.026	−0.219	1.167	0.731
BCP3 [a] (Zr-Cp)	0.042	0.121	0.840	−0.004	−0.096	0.952	1.066 [b]

[a] Averaged properties at the 16 equivalent BCP3 associated with the Zr–C regions. [b] Defined as ∑[DI(Zr-C) + DI(Zr-H(C))].

The source function (SF) provides a measure of the relative importance of each atomic basin's contribution to the density at a reference point, which are usually the CPs. Gatti et al. [34] proposed that the integrated form of the SF provides pertinent chemical information. The percentages of the integrated SF are given in Table 9. These values show that nearly the 66% of the density at the three Zr-O, Zr-P and Zr-Cp interactions is recovered from the Zr involved in such interactions, while about 18% comes from the other Zr. The O, P and Cp basins contribute by about 10% in their respective interactions. This finding contrasts with the traditional conception that in dative or coordinate bonds, most of the partially shared electron density comes from the donor atom.

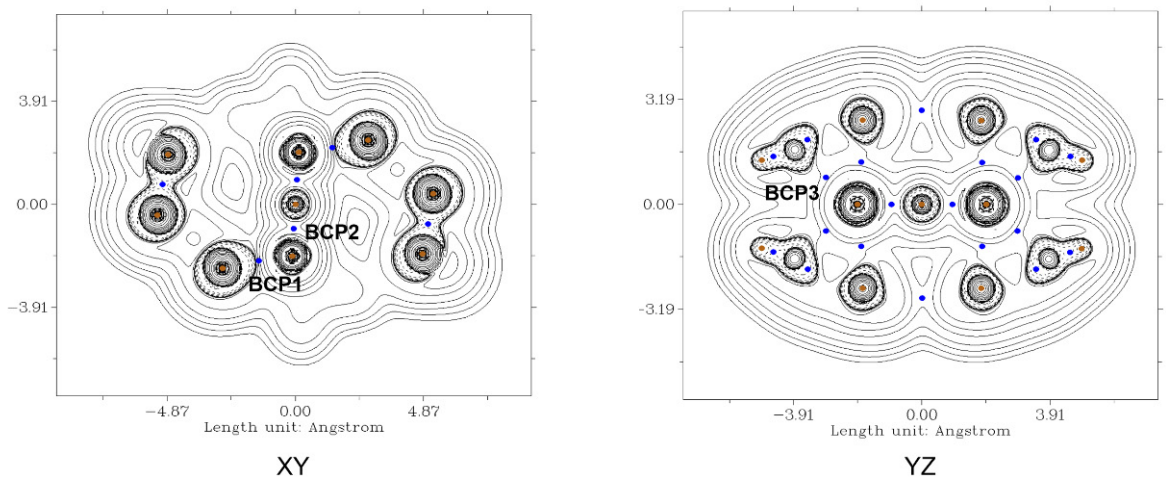

Figure 7. Contour-line maps of the Laplacian of the electron density $\nabla^2\rho_{cp}$ of **1′** on the molecular planes XY and YZ.

Table 9. Percentage contributions to the integrated SF in complex **1′** at BCP1, BCP2 and BCP3 as reference points.

	BCP1 (Zr-P)		BCP2 (Zr-O)		BCP3 (Zr-Cp)	
	SF	**%**	**SF**	**%**	**SF**	**%**
Zr1	0.165	66.5	0.244	66.0	0.158	67.4
Zr2	0.044	17.7	0.067	18.3	0.043	18.2
O	−0.002	-	0.041	11.0	−0.001	-
P	0.023	9.4	0.001	0.3	0.001	0.3
Cp1	0.006	2.2	0.006	1.6	0.027	11.4
Cp2	0.005	2.1	0.006	1.5	0.005	2.1
Total	0.248	97.9	0.370	98.7	0.235	99.3

Finally, the Bader charges were computed and analyzed. The Bader charges are +2.17 (Zr), −1.26 (O), −0.47 (P) and −0.49 (Cp) e. These results suggest the presence of two Zr^{2+} cations, each of them stabilized by one $P^{1/2-}$ phosphorous anion, two $Cp^{1/2-}$ cyclopentadienyl anions and one O^{1-} oxide anion in common.

This QTAIM picture of the bonding pattern of **1′** is not only in complete agreement with the topological analysis of the ELF—which gives no covalent Zr-O and Zr-Cp bonds but only monosynaptic basins associated with the oxygen and Cp rings—but also corrects the misleading disynaptic assignation of the basin found between Zr and P and allows adding valuable, complementary information about the nature of bonding in the regions of interest. Note that in spite of the analogy of dative bonds with covalent bonds, the former are distinguished by their significant polarity, lesser strength and greater length, in such a way that the electron density mostly belongs to one of the two atoms involved. It is worth emphasizing, however, that while the ELF monosynaptic basins belong to the O, P and C(Cp) atoms, the percentage contributions to the integrated SF indicate that the electron density in the regions between those atoms and Zr comes mainly from the metal.

3. Materials and Methods

3.1. Synthesis

A standard Schlenk technique and an inert atmosphere (argon) were employed for the synthesis and subsequent manipulations. Toluene and THF were dried over Na/benzophenone and distilled under nitrogen. A solution of $(Et_2N)_2PPSiMe_3Li$ [35] (1 mmol) in THF was added to $CpCp^*ZrCl_2$ [36] (0.5 mmol) in THF. The mixture turned initially dark red and rapidly discolored. Solvent was evaporated under vacuum, dry residue was dissolved in pentane and LiCl was filtered. This pentane solution was concentrated, and after several days at −70 °C, a small amount of red crystals of compound

1 was deposited. When the reaction mixture was heated (50 °C, 4 h) the yield of isolated compound **1** increased (yield: 5–10%). The attempts to study compound **1** with NMR in solution did not succeed because of low solubility of this compound. Compound **1** is extremely sensitive and easily hydrolyzes on air. Elemental analysis and IR spectra are included in the Supplementary Materials.

3.2. X-ray Crystallography

Experimental diffraction data were collected on a KM4CCD kappa-geometry diffractometer, equipped with a Sapphire2 CCD detector. An enhanced X-ray MoKα radiation source with a graphite monochromator was used. Determination of the unit cells and data collection were carried out at 298 K. Data reduction, absorption correction, space group determination, solution and refinement were performed using the CRYSALISPRO software package [37]. The structures were solved by direct methods and refined by full-matrix least-squares on F^2 (all data) using the SHELXL program package [38].

Crystallographic data for the structure reported here have been deposited with the Cambridge Crystallographic Data Centre (deposition no. CCDC-1059036). These data can be obtained free of charge via http://www.ccdc.cam.ac.uk/perl/catreq.cgi (accessed on 4 October 2021) (or from the CCDC, 12 Union Road, Cambridge CB2 1EZ, U.K.; Fax: (+44) 1223-336-033; e-mail: deposit@ccdc.cam.ac.uk).

3.3. Computational

DFT calculations were performed with the Gaussian 16 suite of programs [39], using the hybrid ωB97X-D functional [40] together with the Def2TZV triple zeta valence basis set [41] and a singlet electronic configuration. The Berny method was used in optimizations [42,43].

The topology of the ELF [21] of the ωB97X-D/Def2TZV monodeterminantal wavefunctions was carried out using the TopMod [44] package with a cubical grid of step size of 0.1 Bohr, while QTAIM [23,24] analysis and ELF color-filled maps were performed using Multiwfn software [45]. The GaussView program [46] was used to visualize molecular geometries and ELF attractor positions.

4. Conclusions

In summary, we obtained and determined the X-ray structure of [{(η^5-C_5H_5)$_2$Zr[P(μ-PNEt$_2$)$_2$P(NEt$_2$)$_2$P]}]$_2$O. This compound was obtained in a reaction of Cp*CpZrCl$_2$ with (Et$_2$N)$_2$PPSiMe$_3$(Li) in THF. We want to stress that complexes which bound phosphetane groups via phosphorus–transition metal bonds are extremely rare.

The theoretical calculations are in agreement with experimental data and show that the interactions involving the Zr metal in the main motif of crystal **1** can be characterized as dative, coordinate bonds in which the non-bonding electron density mainly belongs to the donor (O^{1-}, $P^{1/2-}$ or $Cp^{1/2-}$) anions. Interestingly, the partially shared electron density in the Zr-O, Zr-P and Zr-Cp coordinate bonds mainly comes from the acceptor Zr^{2+} metal cations, increasing the covalent character in the order Zr-Cp < Zr-O < Zr-P. This bonding pattern revealed by QCT methodology suggests that the electronic structure of this type of metal complexes differs from the usual conception based on covalent M-X bonds.

Supplementary Materials: The following are available online. Physical characteristics of complex 1 (elemental analysis and IR spectrum). Table S1: Crystal X-ray diffraction data for complex 1.

Author Contributions: A.Ł.-K.: Methodology, writing and editing; K.K. and J.P.: Writing; M.R.-G.: Formal analysis. All authors have read and agreed to the published version of the manuscript.

Funding: This research was funded by the Ministerio de Ciencias, Innovación y Universidades of the Spanish Government, project PID2019-110776GB-I00 (AEI/FEDER, UE), by PL-Grid Infrastructure in the regional computer center "Cyfronet" in Krakow and by the European Union's Horizon 2020 research and innovation programme under the Marie Skłodowska-Curie grant agreement no. 846181 (MRG).

Institutional Review Board Statement: Not applicable.

Informed Consent Statement: Not applicable.

Data Availability Statement: Data are contained within the article or Supplementary Materials.

Acknowledgments: The authors acknowledge the Ministerio de Ciencias, Innovación y Universidades of the Spanish Government, the PL-Grid Infrastructure in the regional computer center "Cyfronet" in Krakow, the European Commission and the University of Valencia and the Gdansk and Krakow Universities of Technology. Mgr. inż. Przemysław Woliński is also gratefully acknowledged for assisting with calculations when computational resources were unavailable.

Conflicts of Interest: The authors declare no competing interests.

Sample Availability: Not available.

References

1. Liu, J.-Y.; Liu, S.-R.; Li, B.-X.; Li, Y.-G.; Li, Y.-S. Synthesis and Characterization of Novel Half-Metallocene-Type Group IV Complexes Containing Phosphine Oxide–Phenolate Chelating Ligands and Their Application to Ethylene Polymerization. *Organometallics* **2011**, *30*, 4052–4059. [CrossRef]
2. Gibson, V.C.; Spitzmesser, S.K. Advances in Non-Metallocene Olefin Polymerization Catalysis. *Chem. Rev.* **2003**, *103*, 283–316. [CrossRef]
3. Jayaratne, K.C.; Sita, L.R. Stereospecific Living Ziegler−Natta Polymerization of 1-Hexene. *J. Am. Chem. Soc.* **2000**, *122*, 958–959. [CrossRef]
4. Nomura, K.; Liu, J.; Padmanabhan, S.; Kitiyanan, B. Nonbridged Half-Metallocenes Containing Anionic Ancillary Donor Ligands: New Promising Candidates as Catalysts for Precise Olefin Polymerization. *J. Mol. Catal. A Chem.* **2007**, *267*, 1–29. [CrossRef]
5. Ye, K.-Y.; Wang, X.; Daniliuc, C.G.; Kehr, G.; Erker, G. A Ferrocene-Based Phosphane/Borane Frustrated Lewis Pair for Asymmetric Imine Reduction. *Eur. J. Inorg. Chem.* **2017**, *2017*, 368–371. [CrossRef]
6. Naota, T.; Takaya, H.; Murahashi, S.-I. Ruthenium-Catalyzed Reactions for Organic Synthesis. *Chem. Rev.* **1998**, *98*, 2599–2660. [CrossRef] [PubMed]
7. Chen, X.; Nguyen, T.T.D.; Khan, M.Y.; Xia, L.; He, D.; Lee, S.W.; Noh, S.K. Evolution of Ppm Amount of Ru(III) Complexes for Effective Living Radical Polymerization of MMA. *J. Polym. Sci. Part A Polym. Chem.* **2015**, *53*, 1961–1965. [CrossRef]
8. Metters, O.J.; Flynn, S.R.; Dowds, C.K.; Sparkes, H.A.; Manners, I.; Wass, D.F. Catalytic Dehydrocoupling of Amine–Boranes Using Cationic Zirconium(IV)–Phosphine Frustrated Lewis Pairs. *ACS Catal.* **2016**, *6*, 6601–6611. [CrossRef]
9. Flynn, S.R.; Metters, O.J.; Manners, I.; Wass, D.F. Zirconium-Catalyzed Imine Hydrogenation via a Frustrated Lewis Pair Mechanism. *Organometallics* **2016**, *35*, 847–850. [CrossRef]
10. Pikies, J.; Baum, E.; Matern, E.; Chojnacki, J.; Grubba, R.; Robaszkiewicz, A. A New Synthetic Entry to Phosphinophosphinidene Complexes. Synthesis and Structural Characterisation of the First Side-on Bonded and the First Terminally Bonded Phosphinophosphinidene Zirconium Complexes [μ-(1,2:2-η- t Bu 2 P=P){Zr(Cl)Cp 2 } 2] and [{Zr(PPhMe 2)Cp 2}(η 1-P–P t Bu 2)]. *Chem. Commun.* **2004**, *98*, 2478–2479. [CrossRef]
11. Wiśniewska, A.; Łapczuk-Krygier, A.; Baranowska, K.; Chojnacki, J.; Matern, E.; Pikies, J.; Grubba, R. Formation of Polyphosphorus Ligands Mediated by Zirconium and Hafnium Complexes. *Polyhedron* **2013**, *55*, 45–48. [CrossRef]
12. Grubba, R.; Wiśniewska, A.; Baranowska, K.; Matern, E.; Pikies, J. Syntheses and Structures of the First Terminal Phosphanylphosphido Complex of Hafnium [Cp2Hf(Cl){η(1)-(Me3Si)P-P(NEt2)2}] and the First Zirconocene-Phosphanylphosphinidene Dimer [Cp2Zr{μ(2)-P-P(NEt2)2}2ZrCp2]. *Dalton Trans.* **2011**, *40*, 2017–2024. [CrossRef]
13. Łapczuk-Krygier, A.; Baranowska, K.; Ponikiewski, Ł.; Matern, E.; Pikies, J. π-Indenyl Substituted Zirconium Compounds Containing Terminal Bonded Phosphanylphosphido Ligands [Ind2Zr(Cl){(Me3Si)P–PR2-KP1}]. Synthesis, X-Ray Analysis and NMR Studies. *Inorganica Chim. Acta* **2012**, *387*, 361–365. [CrossRef]
14. Lapczuk-Krygier, A.; Baranowska, K.; Pikies, J. 2,4-Bis[Bis(Diisopropyl-Amino)-Phos-Phanyl]-1,2,3,4-Tetra-Phospha-Bicyclo [1.1.0]Butane. *Acta Crystallogr. Sect. E. Struct. Rep. Online* **2008**, *64*, o2427. [CrossRef] [PubMed]
15. Grubba, R.; Kaniewska, K.; Ponikiewski, Ł.; Cristóvão, B.; Ferenc, W.; Dragulescu-Andrasi, A.; Krzystek, J.; Stoian, S.A.; Pikies, J. Synthetic, Structural, and Spectroscopic Characterization of a Novel Family of High-Spin Iron(II) [(β-Diketiminate)(Phosphanyl phosphido)] Complexes. *Inorg. Chem.* **2017**, *56*, 11030–11042. [CrossRef]
16. Petersen, J.L. Preparation and Structural Characterization of [(H5-C5H5)2Zr(SC6H5)]2O. A Qualitative Description of the Bonding in Oxo-Bridged Dicyclopentadienyl-Transition Metal Dimers. *J. Organomet. Chem.* **1979**, *166*, 179–192. [CrossRef]
17. Vivian Wing-Wah, Y.; Qi, G.-Z.; Cheung, K.-K. Synthesis of Luminescent Zirconium Thiolate Complexes. Crystal Structures of (H5-C5H5)2Zr(SC6H4Cl-p)2 and [(H5-C5H5)2Zr(SC6H4OMe-p)]2O. *J. Organomet. Chem.* **1997**, *548*, 289–294. [CrossRef]
18. Stojcevic, G.; Kim, H.; Taylor, N.J.; Marder, T.B.; Collins, S. Methacrylate Polymerization Using a Dinuclear Zirconocene Initiator: A New Approach for the Controlled Synthesis of Methacrylate Polymers. *Angew. Chemie Int. Ed.* **2004**, *43*, 5523–5526. [CrossRef]

19. Klouras, N.; Tzavellas, N.; Raptopoulou, C.P. New Zirconocene Pseudohalogeno Complexes. Crystal Structure of Oxo-Bis[Bis(Cyclopentadienyl)Isocyanatozirconium(IV)], [{Zr(H5-C5H5)2(NCO)}2O]. *Z. Anorg. Allg. Chem.* **1997**, *623*, 1027–1031. [CrossRef]
20. Popelier, P.L.A. On Quantum Chemical Topology. In *Applications of Topological Methods in Molecular Chemistry. Challenges and Advances in Computational Chemistry and Physics*; Chauvin, R., Lepetit, C., Silvi, B., Alikhani, E., Eds.; Springer: Cham, Switzerland, 2016; pp. 23–52.
21. Becke, A.D.; Edgecombe, K.E. A Simple Measure of Electron Localization in Atomic and Molecular Systems. *J. Chem. Phys.* **1990**, *92*, 5397–5403. [CrossRef]
22. Bader, R.F.W.; Essén, H. The Characterization of Atomic Interactions. *J. Chem. Phys.* **1983**, *80*, 1943–1960. [CrossRef]
23. Popelier, P.L.A. *The QTAIM Perspective of Chemical Bonding*; Wiley: Hoboken, NJ, USA, 2014; Volume 9783527333, ISBN 9783527664696.
24. Vener, M.V.; Manaev, A.V.; Egorova, A.N.; Tsirelson, V.G. QTAIM Study of Strong H-Bonds with the O-H· · · A Fragment (A = O, N) in Three-Dimensional Periodical Crystals. *J. Phys. Chem. A* **2007**, *111*, 1155–1162. [CrossRef] [PubMed]
25. Bader, R.F.W. *Atoms in Molecules A Quantum Theory*; Clarendon Press: Oxford, UK, 1994; ISBN 0198558651.
26. Gatti, C. Chemical Bonding in Crystals: New Directions. *Z. Krist.* **2005**, *220*, 399–457. [CrossRef]
27. Espinosa, E.; Alkorta, I.; Elguero, J.; Molins, E. From Weak to Strong Interactions: A Comprehensive Analysis of the Topological and Energetic Properties of the Electron Density Distribution Involving X-H· · · F-Y Systems. *J. Chem. Phys.* **2002**, *117*, 5529–5542. [CrossRef]
28. Silvi, B. The Synaptic Order: A Key Concept to Understand Multicenter Bonding. *J. Mol. Struct.* **2002**, *614*, 3–10. [CrossRef]
29. Grabowski, S.J. What Is the Covalency of Hydrogen Bonding? *Chem. Rev.* **2011**, *111*, 2597–2625. [CrossRef] [PubMed]
30. Gervasio, G.; Bianchi, R.; Marabello, D. About the Topological Classification of the Metal-Metal Bond. *Chem. Phys. Lett.* **2004**, *387*, 481–484. [CrossRef]
31. Bader, R.F.W. A Quantum Theory of Molecular Structure and Its Applications. *Chem. Rev.* **1991**, *91*, 893–928. [CrossRef]
32. Ivanov, Y.; Nimura, T.; Tanaka, K. Electron Density and Electrostatic Potential of KMnF3: A Phase-Transition Study. *Acta Crystallogr. Sect. B Struct. Sci.* **2004**, *60*, 359–368. [CrossRef]
33. Tsirelson, V.; Abramov, Y.; Zavodnik, V.; Stash, A.; Belokoneva, E.; Stahn, J.; Pietsch, U.; Feil, D. Critical Points in a Crystal and Procrystal. *Struct. Chem.* **1998**, *9*, 249–254. [CrossRef]
34. Gatti, C.; Cargnoni, F.; Bertini, L. Chemical Information from the Source Function. *J. Comput. Chem.* **2003**, *24*, 422–436. [CrossRef]
35. Kovacs, I.; Matern, E.; Fritz, G. Zum Einfluß Der Substituenten R = Ph, NEt2,IPr UndtBu in Triphosphanen, (R2P)2P?SiMe3, Und Phosphiden, Li(THF)2[(R2P)2P], Auf Die Bildung Und Eigenschaften von Phosphinophosphiniden-Phosphoranen. *Z. Anorg. Allg. Chem.* **1996**, *622*, 935–941. [CrossRef]
36. Wolczanski, P.T.; Bercaw, J.E. Alkyl and Hydride Derivatives of (Pentamethylcyclopentadienyl)Zirconium(IV). *Organometallics* **1982**, *1*, 793–799. [CrossRef]
37. *Program CRYSALISPRO*; Version 1.171; Oxford Diffraction: Abingdon, UK, 2008.
38. Sheldrick, G.M. A Short History of SHELX. *Acta Crystallogr. A.* **2008**, *64*, 112–122. [CrossRef] [PubMed]
39. Reed, A.E.; Weinstock, R.B.; Weinhold, F. Natural Population Analysis. *J. Chem. Phys.* **1985**, *83*, 735–746. [CrossRef]
40. Da Chai, J.; Head-Gordon, M. Long-Range Corrected Hybrid Density Functionals with Damped Atom-Atom Dispersion Corrections. *Phys. Chem. Chem. Phys.* **2008**, *10*, 6615–6620. [CrossRef]
41. Schäfer, A.; Horn, H.; Ahlrichs, R. Fully Optimized Contracted Gaussian Basis Sets for Atoms Li to Kr. *J. Chem. Phys.* **1992**, *97*, 2571–2577. [CrossRef]
42. Schlegel, H.B. Optimization of Equilibrium Geometries and Transition Structures. *Adv. Chem. Phys.* **2007**, *67*, 249–286. [CrossRef]
43. Schlegel, H.B. *Modern Electronic Structure Theory*; Yarkony, D.R., Ed.; World Scientific Publishing: Singapore, 1994; ISBN 978-9810229870.
44. Noury, S.; Krokidis, X.; Fuster, F.; Silvi, B. Computational Tools for the Electron Localization Function Topological Analysis. *Comput. Chem.* **1999**, *23*, 597–604. [CrossRef]
45. Lu, T.; Chen, F. Multiwfn: A Multifunctional Wavefunction Analyzer. *J. Comput. Chem.* **2012**, *33*, 580–592. [CrossRef]
46. Dennington, R.; Keith, T.; Millam, J. *GaussView Version 6.0*; Semichem Inc.: Shawnee, KS, USA, 2016.